Construction and Building Materials 82 (2015) 61–70

Contents lists available at ScienceDirect

Construction and Building Materials

journal homepage: www.elsevier.com/locate/conbuildmat

Influence of concrete age on stress–strain behavior of FRP-confined normal- and high-strength concrete

Jian C. Lim, Togay Ozbakkaloglu *

School of Civil, Environmental and Mining Engineering, University of Adelaide, Australia

HIGHLIGHTS

- Influence of concrete age on compressive behavior of FRP-confined concrete was investigated.
- Transition zone of stress–strain curve of FRP-confined concrete changes with concrete age.
- Dilation behavior of FRP-confined concrete changes with concrete age.
- Strength and strain enhancements decrease slightly with an increase in concrete age.
- Hoop rupture strain of FRP jacket also decreases with an increase in concrete age.

ARTICLE INFO

Article history:
Received 13 August 2014
Received in revised form 14 January 2015
Accepted 18 February 2015
Available online 6 March 2015

Keywords:
Concrete
High-strength concrete (HSC)
Fiber reinforced polymer (FRP)
Confinement
Compression
Age
Stress–strain relations

ABSTRACT

The potential applications of fiber reinforced polymer (FRP) composites as concrete confinement in retrofitting existing concrete columns and in the construction of new high-performance composite columns have received significant research attention. In practical applications, the ages of concrete in retrofitted columns are significantly different from those of newly constructed columns. Without a full understanding on the influence of concrete age on their compressive behaviors, the validity of existing experimental findings, which are based the age of concrete at the time of testing, remains ambiguous when the design application lapses in time. This paper presents the results of an experimental study on the influence of concrete age on the compressive behavior of FRP-confined normal-strength (NSC) and high-strength concrete (HSC). The first part of the paper presents the results of 18 FRP-confined and 18 unconfined concrete specimens tested at 7 and 28 days. To extend the investigation with specimens with concrete ages up to 900 days, existing test results of FRP-confined concrete was assembled from the review of the literature. Based on observations from both short- and long-term influences of concrete age on compressive behavior of FRP-confined concrete, a number of important findings were drawn and are presented in the second part of the paper. It was observed that, at a same level of FRP confinement and unconfined concrete strength, the stress–strain behavior of FRP-confined concrete changes with concrete age. This difference is particularly pronounced at the transition zone of the stress–strain curves. It is found that, in the short-term, the ultimate condition of FRP-confined concrete is not significantly affected by the age of concrete. However, in the long-term, slight decreases in the compressive strength and the ultimate axial strain are observed with an increase in concrete age.

1. Introduction

Understanding the influence of concrete age on the compressive behavior of FRP-confined concrete in newly constructed and retrofitted existing columns is of vital importance. A number of existing studies have investigated time-related issues affecting the compressive behavior of FRP-confined concrete under various environmental exposures [1–6] and sustained loading [7–12]. However, none of these studies directly investigated the influence of concrete age on the stress–strain behavior of FRP-confined concrete. To gain an insight into the possible changes in the behavior of FRP-confined concrete members throughout their service lives, influence of concrete age on the stress–strain behavior of FRP-confined concrete needs to be understood. To this end, the experimental program reported in the present study investigated the axial compressive behaviors of 18 FRP-confined and 18 unconfined NSC and HSC specimens tested at 7 or 28 days of concrete age.

* Corresponding author. Tel.: +61 8 8313 6477; fax: +61 8 8313 4359.
E-mail address: togay.ozbakkaloglu@adelaide.edu.au (T. Ozbakkaloglu).

http://dx.doi.org/10.1016/j.conbuildmat.2015.02.020
0950-0618/

The specimens were prepared such that concretes at different ages attained the same unconfined strength at the day of testing and they were confined with the same amount of FRP. To extend the observation range of concrete age up to 900 days, the results of the present study were analyzed together with those from several groups of specimens assembled from the published literature.

2. Experimental program

2.1. Test specimens and materials

18 FRP-confined and 18 unconfined concrete cylinders were prepared. All of the specimens were 152.5 mm in diameter and 305 mm in height. The influence of concrete age on the mechanical properties of the confined and unconfined specimens was investigated using six separate batches of concrete mixes. The mixes were designed such that, in each comparison pair, companion specimens tested at 7 and 28 days developed the same test-day unconfined concrete strength. The mix proportions of each batch of concrete is given in Table 1. Crushed bluestone gravel of 7 mm maximum size and graded sand were used as the aggregates. The specimens were manufactured using concrete mixes of two different grades, namely HSC and NSC. The HSC specimens in Batches 1–4 had an average strength of 73.0 MPa and the NSC specimens in Batches 5 and 6 had an average strength of 33.9 MPa. To establish the final w/c ratios used in Batches 1–6, a large number of trial batches were prepared and tested. The summary of the axial compression test results of the unconfined specimens are given in Table 2, which provides the peak stress (f'_{co}) and corresponding axial strain (ε_{co}) of the specimens. The axial strain corresponding to the peak stress of unconfined concrete (ε_{co}) was not recorded during the compression tests, and values reported in Table 2 were calculated using the expression proposed by Lim and Ozbakkaloglu [13].

$$\varepsilon_{co} = \frac{f'^{\,0.225k_d}_{co}}{1000} k_s k_a \quad (1)$$

where f'_{co} is in MPa, and k_d, k_s, and k_a, respectively, are the coefficients to allow for concrete density, specimens size and specimen aspect ratio. Each of these coefficients becomes unity for a specimen with concrete density of 2400 kg/m^3, diameter of 152 mm and height of 305 mm, as was the case for the control cylinders of the present study.

A total of 18 FRP tubes were prepared using a manual wet lay-up process by wrapping epoxy resin impregnated unidirectional fiber sheets around precision-cut high-density Styrafoam templates, which were removed prior to concrete casting. The FRP tubes were prepared using a single continuous fiber sheet and had a single 150-mm long overlap region. The material properties of the aramid and S-glass fiber sheets used to manufacture the FRP tubes are provided in Table 3. The table reports both the manufacturer-supplied fiber properties and the tensile tested FRP composite properties. The tensile properties of the FRP made from these fiber sheets were determined from flat coupon tests, where the loading was applied in accordance with ASTM D3039 [14].

The FRP tubes of the 12 specimens were manufactured using S-glass FRP (GFRP), and the tubes of the remaining six specimens were manufactured with aramid FRP (AFRP). The specimens with AFRP tubes and six of the specimens with GFRP tubes were cast with HSC, whereas the remaining six GFRP tube encased specimens were manufactures using NSC. The tubes of NSC and HSC specimens had two and four layers of FRP, respectively. These FRP layer arrangements were determined based on the understanding that the confinement demand of concrete increases with its strength [15–18]. Three nominally identical specimens were tested for each unique specimen configuration. The FRP-confined specimens were tested on the same day with their companion unconfined specimens, through which the test-day unconfined concrete strengths (f'_{co}) reported in Table 2 were established.

Table 1
Mix proportions of concrete specimens tested at different ages.

Designated study	AFRP tube-encased HSC		GFRP tube-encased HSC		GFRP tube-encased NSC	
Batch	B1	B2	B3	B4	B5	B6
Cement (kg/m^3)	550	520	550	520	380	380
Sand (kg/m^3)	710	710	710	710	710	710
Gravel (kg/m^3)	1065	1065	1065	1065	1065	1065
Water (kg/m^3)	133	137	133	137	213	243
Superplasticiser (kg/m^3)	20	20	20	20	0	0
Water–cementitious binder ratio	0.270	0.294	0.270	0.294	0.560	0.640
Slump height (m)	>0.250	>0.250	>0.250	>0.250	0.065	0.190
Concrete age at testing (day)	7	28	7	28	7	28

Table 2
Compression test results of unconfined specimens.

Specimen	Concrete batch	Age (day)	w/c ratio (%)	Avg. f'_{co} (MPa)	Avg. ε_{co}[a] (%)
A0-U73-D7	B1	7	0.27	72.0	0.26
A0-U73-D28	B2	28	0.29	74.9	0.26
G0-U73-D7	B3	7	0.27	70.8	0.26
G0-U73-D28	B4	28	0.29	74.1	0.26
G0-U34-D7	B5	7	0.56	33.0	0.22
G0-U34-D28	B6	28	0.64	34.7	0.22

[a] Axial strains were not recorded experimentally. Values determined using expression given by Lim and Ozbakkaloglu [13].

2.2. Specimen designation

The specimens in Tables 2 and 4 were labeled as follows: the first letter A, G or C represents the type of FRP (i.e., AFRP, GFRP or CFRP) and it is followed by the number of FRP layer; the second letter U is followed by the unconfined concrete strength in MPa; and the third letter D is followed by the age of concrete in days at the day of testing. Finally, the last number in the specimen designation (i.e., 1, 2 or 3) was used to make the distinction between three nominally identical specimens. For instance, A4-C73-D7-2 represents the second of the three nominally identical specimens, which were tested at 7 days of concrete age were and cast from a concrete mix with a 73 MPa unconfined concrete strength in an FRP tube manufactured with 4 layers of aramid fibers.

2.3. Instrumentation and testing

The specimens were tested under axial compression using a 5000-kN capacity universal testing machine. During the initial elastic stage of the behavior, the loading was applied with the load control set at 5 kN per second, whereas displacement control operated at 0.004 mm per second beyond the initiation of transition region until specimen failure. Prior to testing, all specimens were ground at both ends to ensure uniform distribution of the applied pressure, and load was applied directly to the concrete core using precision-cut high-strength steel plates with a 150 mm diameter.

The hoop strains of the specimens were measured using 12 unidirectional strain gauges placed at the mid-height around the circumference of specimens outside the overlap region. As illustrated in Fig. 1, the axial strains of the confined specimens were measured using two different methods: (i) four linear variable displacement transformers (LVDTs) mounted at each corner of the steel loading platens with a gauge length of 305 mm; and (ii) four LVDTs placed at the mid-height at a gauge length of 175 mm at 90° spacing along the circumference of specimens. The readings from the mid-height LVDTs were used to correct the full-height LVDT measurements at the early stages of loading, where additional displacements due to closure of the gaps in the setup were also recorded by the full-height LVDTs.

3. Test results and discussion

3.1. Failure mode

The typical failure modes of the FRP-confined specimens tested at 7 and 28 days are illustrated in Figs. 2–4. As can be seen from the photos, all of the specimens failed by the rupture of the FRP jackets. As illustrated in Figs. 2(a) and 3(a), heterogenic microcrack formations were observed in the concretes of the 7-day old AFRP- and GFRP-confined HSC specimens at failure. On the other hand, as evident from Figs. 2(b) and 3(b), the concrete in the companion 28-day old specimens exhibited larger cracks that were more localized. In the GFRP-confined NSC specimens shown in Fig. 4(a) and (b), the change in the concrete cracking pattern from microcrack to macrocrack with an increase in concrete age are also evident, however the change is not as pronounced as those seen in the HSC specimens. The observed variations in the cracking patterns of concretes of same compressive strength suggest that the concrete brittleness increases with its age. This change in concrete brittleness with concrete age is more pronounced in higher strength concrete.

Table 3
Material properties of fibers and FRP composites.

Type	Nominal thickness t_f (mm/ply)	Provided by manufacturers			Obtained from flat FRP coupon tests		
		Tensile strength f_f (MPa)	Ultimate tensile strain ε_f (%)	Elastic modulus E_f (GPa)	Tensile strength f_{frp} (MPa)	Ultimate tensile strain ε_{frp} (%)	Elastic modulus E_{frp} (GPa)
Aramid	0.200	2600	2.20	118.2	2390	1.86	128.5
S-glass	0.200	3040	3.50	86.9	3055	3.21	95.3

Table 4
Compression test results of confined specimens tested at different ages.

Specimen	Concrete batch	Age (day)	f'_{cc} (MPa)	ε_{cu} (%)	$\varepsilon_{h,rup}$ (%)	f'_{cc}/f'_{co}	Avg. f'_{cc}/f'_{co}	$\varepsilon_{cu}/\varepsilon_{co}$	Avg. $\varepsilon_{cu}/\varepsilon_{co}$	$k_{\varepsilon,f}$	Avg. $k_{\varepsilon,f}$
A4-U73-D7-1	B1	7	132.4	1.92	1.74	1.84	1.94	7.34	8.11	0.79	0.86
A4-U73-D7-2			145.1	2.30	2.04	2.02		8.79		0.93	
A4-U73-D7-3			140.5	2.15	1.87	1.95		8.21		0.85	
A4-U73-D28-1	B2	28	130.1	1.88	1.65	1.74	1.78	7.12	7.21	0.75	0.81
A4-U73-D28-2			130.5	1.69	1.67	1.74		6.40		0.76	
A4-U73-D28-3			139.3	2.14	2.02	1.86		8.10		0.92	
G4-U73-D7-1	B3	7	126.7	2.51	2.57	1.79	1.77	9.63	9.25	0.73	0.72
G4-U73-D7-2			128.4	2.36	2.44	1.81		9.05		0.70	
G4-U73-D7-3			121.3	2.37	2.57	1.71		9.09		0.73	
G4-U73-D28-1	B4	28	136.0	2.69	2.45	1.84	1.85	10.21	10.17	0.70	0.68
G4-U73-D28-2			138.7	2.74	2.46	1.87		10.40		0.70	
G4-U73-D28-3			136.3	2.61	2.23	1.84		9.91		0.64	
G2-U34-D7-1	B5	7	67.3	3.06	2.72	2.04	2.07	13.93	14.54	0.78	0.80
G2-U34-D7–2			68.7	3.08	2.97	2.08		14.02		0.85	
G2-U34-D7-3			69.3	3.44	2.73	2.10		15.66		0.78	
G2-U34-D28-1	B6	28	78.1	3.39	2.45	2.25	2.20	15.26	15.38	0.70	0.71
G2-U34-D28-2			76.3	3.63	2.48	2.20		16.34		0.71	
G2-U34-D28-3			75.1	3.23	2.49	2.16		14.54		0.71	

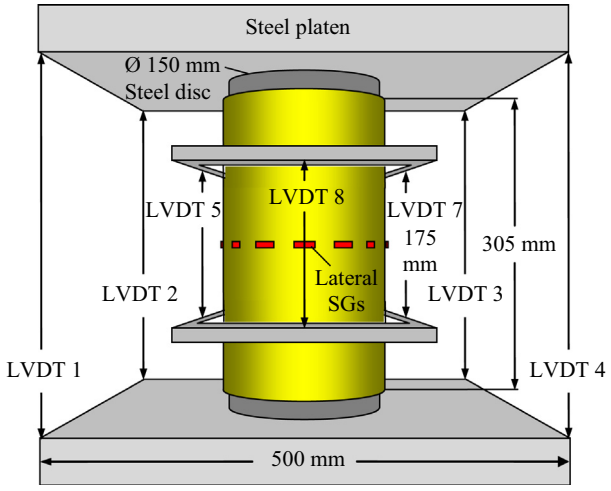

Fig. 1. Test setup and instrumentation.

3.2. Axial stress–strain and lateral strain–axial strain relationships

Fig. 5(a) and (b) illustrate the different stages observed on a typical axial stress–strain curve and the corresponding lateral strain–axial strain curve of the specimens. The different stages marked on these curves were established based on the observed changes in the concrete expansion behavior, which is indicated by different tangential slopes of the corresponding regions shown in Fig. 5(b), namely: linear elastic region, rapid expansion region, and stabilized dilation region. These regions matches the three different portions of the axial stress–strain curves shown in Fig. 5(a), namely: first ascending portion, transition region, and second ascending branch.

The axial stress–strain curves of the AFRP-confined HSC, GFRP-confined HSC, and GFRP-confined NSC specimens are shown in Figs. 6–8, respectively. As illustrated in the figures, the shape of stress–strain curves of both the 7-day and 28-day old specimens initiated with an ascending branch that was followed by a transition region, which connected the initial branch to a nearly straight-line second branch. As evident from the curved segments marked in Figs. 6–8, there were significant differences in the radii of the transition regions of the 7-day and 28-day old specimens. Comparisons of Figs. 6(a) and (b) and 7(a) and (b) indicate that the transition radii of the 7-day old HSC specimens were larger

Fig. 2. Failure modes of AFRP-confined HSC specimens tested at: (a) 7 days; and (b) 28 days.

Fig. 3. Failure modes of GFRP-confined HSC specimens tested at: (a) 7 days; and (b) 28 days.

than those of their 28-day old counterparts. For the NSC specimens, the change in the transition radii with concrete age was less pronounced but can still be seen from the comparison of Fig. 8(a) and (b). The reduction in the transition radius with concrete age can be attributed to the change in the concrete cracking pattern from microcracks to macrocracks, as illustrated earlier in Figs. 2–4.

The resulting influence of the change in concrete cracking pattern on the dilation behavior of concrete can be seen in the lateral strain–axial strain relationships shown in Figs. 9–11. To enable an easier observation of these differences, the segments corresponding to the transition regions on the axial stress–strain curves are also marked on the companion lateral strain–axial strain curves in Figs. 9–11. In addition, the average slope of the marked segment in each figure is indicated by the dash-dotted line. As evident from Figs. 9–11, the curves of the 28-day old specimens exhibited higher tangential slopes within the marked segments compared to the curves of the 7-day old specimens. The increased tangential slope indicates that the concrete dilation rates of the 28-day old specimens are higher at the transition region as a result of the more rapid concrete expansion. This rapid concrete expansion can be attributed to the increased concrete crack size due to the change

Fig. 4. Failure modes of GFRP-confined NSC specimens tested at: (a) 7 days; and (b) 28 days.

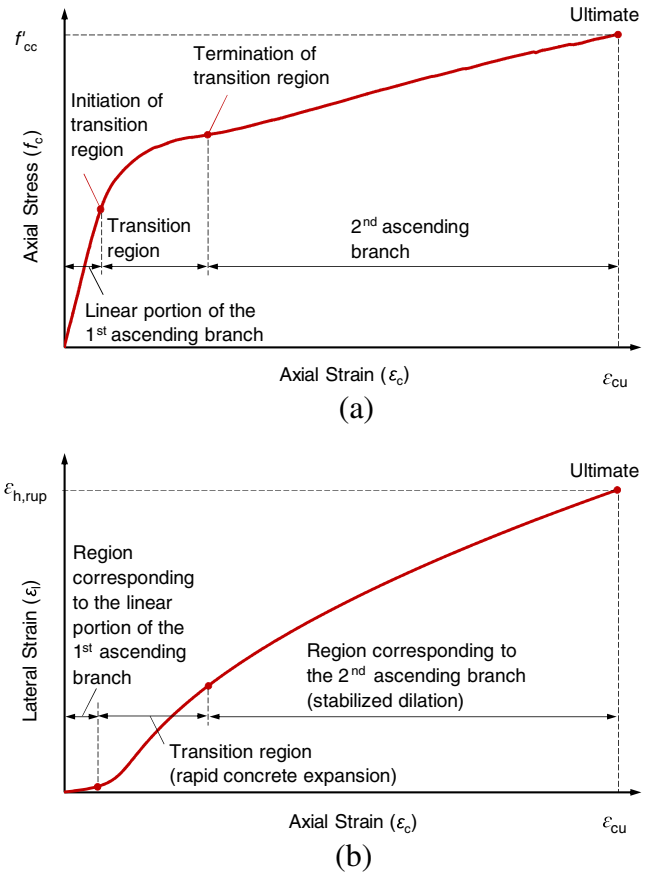

Fig. 5. Illustration of different stages of: (a) axial stress–strain; and (b) lateral strain–axial strain curves of specimen.

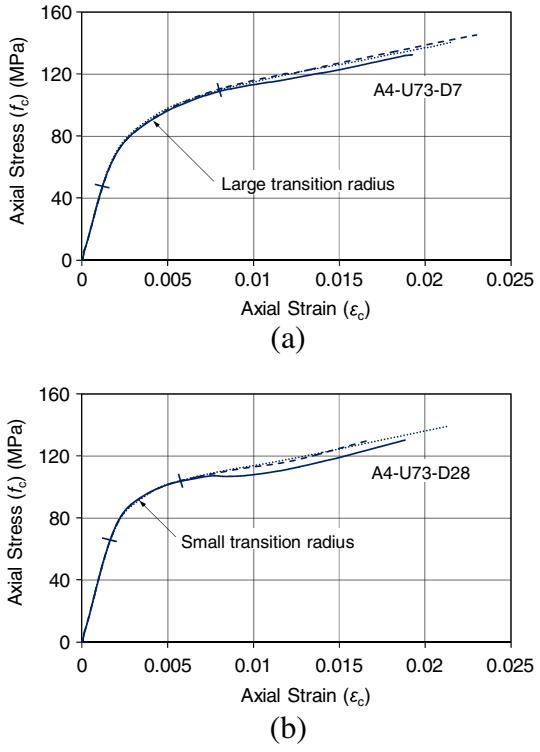

Fig. 6. Axial stress–strain curves of AFRP-confined HSC specimens tested at: (a) 7 days; and (b) 28 days.

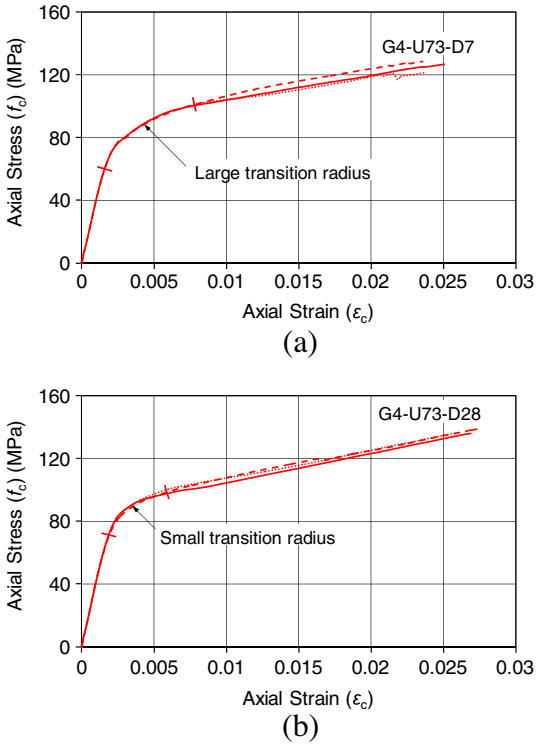

Fig. 7. Axial stress–strain curves of GFRP-confined HSC specimens tested at: (a) 7 days; and (b) 28 days.

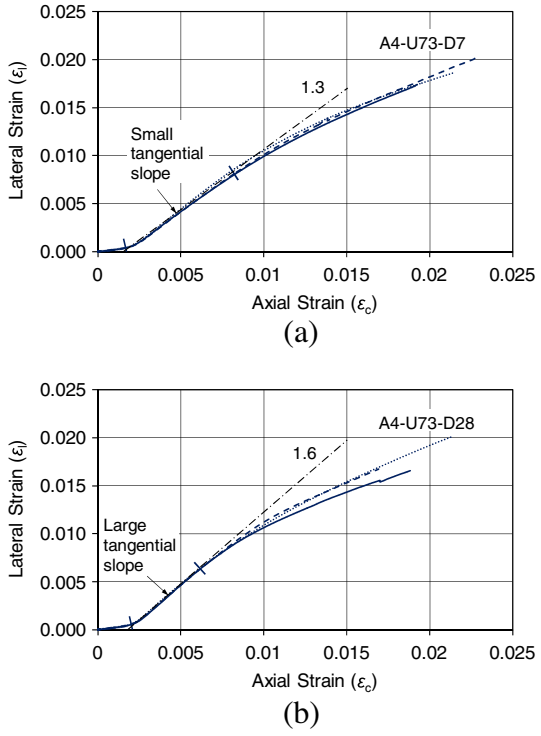

Fig. 9. Lateral strain–axial strain curves of AFRP-confined HSC specimens tested at: (a) 7 days; and (b) 28 days.

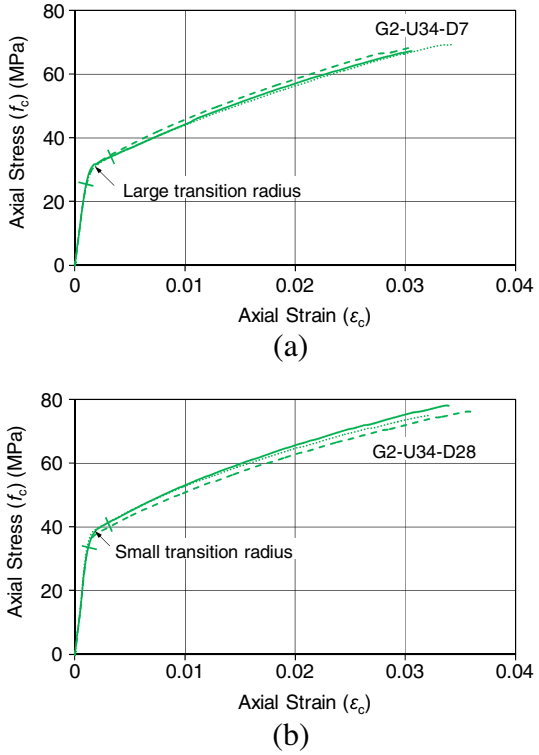

Fig. 8. Axial stress–strain curves of GFRP-confined NSC specimens tested at: (a) 7 days; and (b) 28 days.

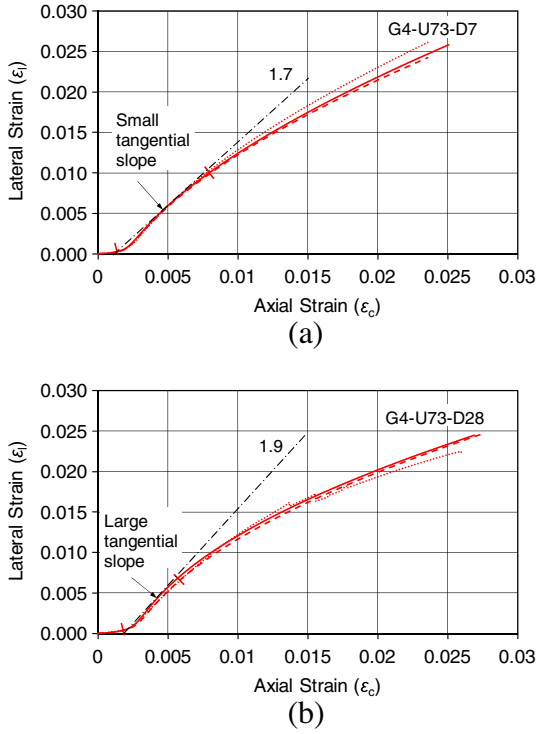

Fig. 10. Lateral strain–axial strain curves of GFRP-confined HSC specimens tested at: (a) 7 days; and (b) 28 days.

in cracking pattern from microcrack to macrocrack formation, as seen earlier from the failure modes of the specimens in Figs. 2–4. It can also be seen from Figs. 9(b) to 11(b) that the 28-day old specimens experienced higher concrete dilation rates as a result of the change in concrete cracking pattern. This increased concrete dilation rates in turn resulted in smaller transition radii of the axial stress–strain curves shown earlier in Figs. 6(b)–8(b). The

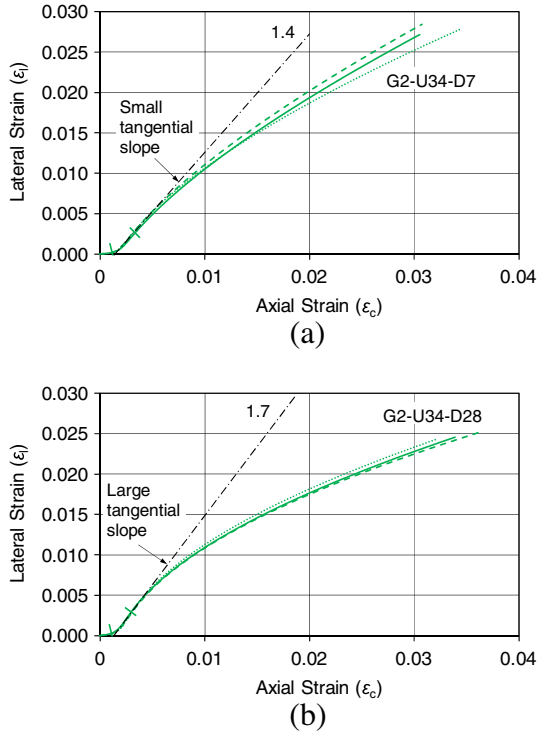

Fig. 11. Lateral strain–axial strain curves of GFRP-confined NSC specimens tested at: (a) 7 days; and (b) 28 days.

observations from Figs. 6 to 11 indicate that, for concretes with the same strength, an increase in concrete age alters the cracking pattern and dilation rate of concrete, which in turn reduces the transition radius of the stress–strain curves.

3.3. Ultimate conditions

The ultimate condition of FRP-confined concrete is often characterized as the ultimate axial stress and strain of concrete recorded at the rupture of the FRP jacket. This makes the relationship between the ultimate axial stress (f'_{cu}), ultimate axial strain (ε_{cu}) and hoop rupture strain ($\varepsilon_{h,rup}$) an important one. The test results of the FRP-confined specimens of the present study are given in Table 4, which include: the concrete age; compressive strength and ultimate axial strain of the specimens (f'_{cc} and ε_{cu}); hoop rupture strain ($\varepsilon_{h,rup}$); strength and strain enhancement ratios (f'_{cc}/f'_{co} and $\varepsilon_{cu}/\varepsilon_{co}$); and hoop strain reduction factor ($k_{\varepsilon,f}$). The hoop strain reduction factor ($k_{\varepsilon,f}$) of the confined specimens was calculated as the ratio of the hoop rupture strain ($\varepsilon_{h,rup}$) to ultimate tensile strain of the fiber (ε_f). The ultimate axial strain of confined concrete (ε_{cu}) reported in Table 4 was averaged from the four steel platen mounted LVDTs, with corrections supplied from the four mid-section LVDTs, as mentioned previously.

3.3.1. Strength and strain enhancements

To illustrate the influence of concrete age on the ultimate condition of FRP-confined concrete, Figs. 12(a) and 13(a) show the variation of the strength and strain enhancement ratios (f'_{cc}/f'_{co} and $\varepsilon_{cu}/\varepsilon_{co}$) with concrete age for specimens of the present study. Comparison of the first two groups of specimens in Figs. 12(a) and 13(a) indicates that both the strength and strain enhancement ratios (f'_{cc}/f'_{co} and $\varepsilon_{cu}/\varepsilon_{co}$) of the 7-day old AFRP-confined HSC specimens were slightly higher than that of their 28-day old counterparts. As opposed to the AFRP-confined specimens, the 7-day old GFRP-confined HSC and NSC specimens had slightly lower strength

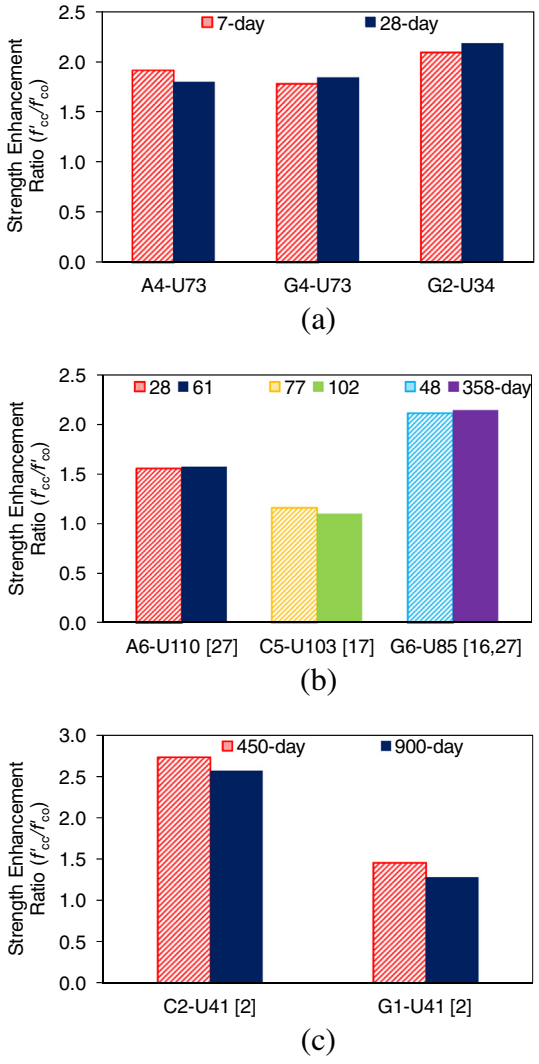

Fig. 12. Variations of strength enhancement ratio (f'_{cc}/f'_{co}) with concrete age: (a) 7–28 days; (b) 28–358 days; and (c) 450–900 days.

and strain enhancement ratios (f'_{cc}/f'_{co} and $\varepsilon_{cu}/\varepsilon_{co}$) than their 28-day old counterparts, as evident from the comparison of the remaining four groups of specimens in Figs. 12(a) and 13(a). To gain further insight into this influence, a large experimental test database that was assembled through an extensive review of the literature [18,19] was also studied in the analysis. Specimen groups were prepared by sorting specimens in the database according to the specimen unconfined concrete strengths, geometrical dimensions, types of FRP material, amount of FRP confinement, and concrete age. These specimen groups, as summarized in Table 5, were sorted such that the concrete age was the only variable with the other parameters remaining nearly constant. The strength and strain enhancement ratios (f'_{cc}/f'_{co} and $\varepsilon_{cu}/\varepsilon_{co}$) of these specimen groups are presented in Figs. 12(b and c) and 13(b and c), respectively. In Fig. 12(b), a slight reduction in the strength enhancement ratios (f'_{cc}/f'_{co}) with concrete age can be seen in the specimen group tested at 77 and 102 days, but no notable change is evident in the specimen groups tested at 28 and 61 days and 48 and 358 days. Fig. 13(b) illustrates that the strain enhancement ratios ($\varepsilon_{cu}/\varepsilon_{co}$) of all of these specimen groups decreased slightly with an increase in concrete age. Furthermore, as can be seen in Figs. 12(c) and 13(c), both the strength and strain enhancement ratios (f'_{cc}/f'_{co} and $\varepsilon_{cu}/\varepsilon_{co}$) decreased with an increase in concrete age from 450 and 900 days.

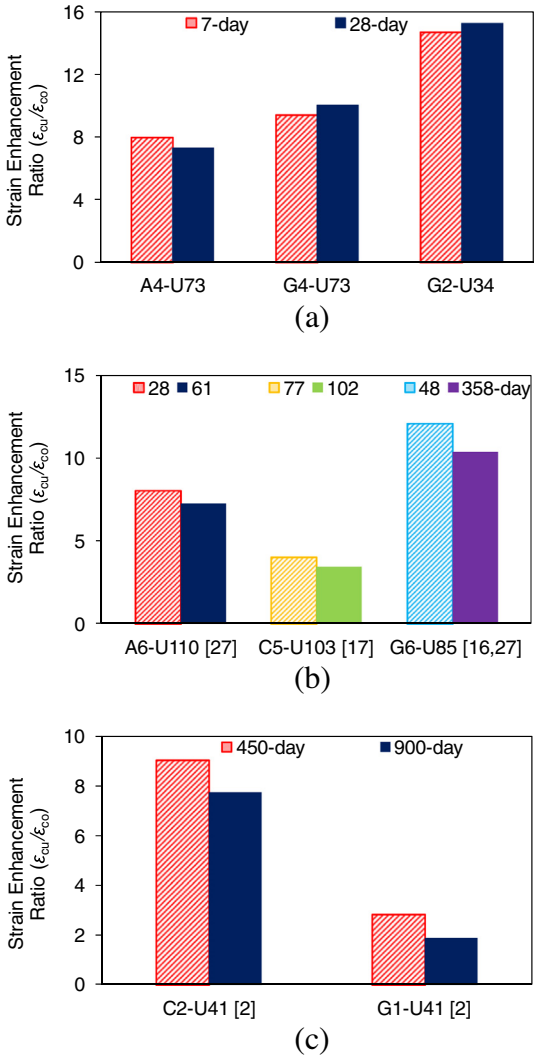

Fig. 13. Variations of strain enhancement ratio ($\varepsilon_{cu}/\varepsilon_{co}$) with concrete age: (a) 7–28 days; (b) 28–358 days; and (c) 450–900 days.

These observations indicate that, for specimens with up to 28 days of concrete age, the concrete age does not have a notable influence on the ultimate condition of FRP-confined concrete, and the slight differences observed in the test results appears to be mainly a margin of scatter among the results of different specimen groups. On the other hand, the results suggest that the strength and strain enhancements seen in FRP-confined concrete tends to decrease with an increase in concrete age for specimens with concrete ages of over 450 days. This effect is less pronounced for specimens with concrete ages between 28 and 450 days.

To validate the observed influence of concrete age on the ultimate condition of FRP-confined concrete, the results in the large experimental test database [18,19] was further studied. Out of 1063 available results, 339 and 329 datasets that were reported with concrete age details were used respectively to investigate the influence of concrete age on compressive strength (f'_{cc}) and ultimate axial strain (ε_{cu}). Fig. 14(a) and (b), respectively, show the observed variations in the strength and strain enhancement coefficients (k_1 and k_2) with concrete age (d). The strength and strain enhancement coefficients (k_1 and k_2) shown in Fig. 14, which represent the level of increase in the compressive strength (f'_{cc}) and ultimate axial strain (ε_{cu}) with an increase in the level of confinement, were calculated using the model proposed by Ozbakkaloglu and Lim [18]. As can be seen in Fig. 14, both k_1 and k_2 exhibit trendlines with a very shallow descending slope. As a result, the ultimate condition of FRP-confined concrete is not particularly sensitive to the variation in the concrete age in the short-term. However, the said trend results in slightly lower compressive strengths and ultimate axial strains of specimens with higher concrete ages when the longer term behavior is considered.

3.3.2. Hoop strain reduction

It has been discussed previously in a number of studies [15–18,20–25] that the ultimate hoop strain ($\varepsilon_{h,rup}$) reached in the FRP jacket is often smaller than the ultimate tensile strain of the fibers (ε_f), which necessitates the use of a strain reduction factor ($k_{\varepsilon,f}$) in the determination of the actual confining pressures. The recorded hoop rupture strains ($\varepsilon_{h,rup}$) and calculated strain reduction factors (i.e., $k_{\varepsilon,f} = \varepsilon_{h,rup}/\varepsilon_f$) of the specimens in the present study are provided in Table 4. It was recently demonstrated by the authors that the hoop rupture strain of FRP jacket reduces with an increase in the concrete strength [15,18,26]. A similar phenomenon was observed in the specimens of the current study, which is evident from the comparison of the results of the 28-day old GFRP-confined HSC and NSC specimens (Batches B4 and B6) that shows a reduction in the recorded $k_{\varepsilon,f}$ values with an increase in unconfined concrete strength (f'_{co}).

The results shown in Table 4 also indicate that the hoop rupture strain of FRP jacket is influenced by the age of concrete. Fig. 15 shows the variation of $k_{\varepsilon,f}$ values with concrete age of the specimen groups tested in the present and the existing studies [2,16,17,27]. As illustrated in Fig. 15(a), the test results of the 7-day and 28-day old specimens with comparable unconfined concrete strength (f'_{co}) show that $k_{\varepsilon,f}$ decreased with an increase in concrete age. This reduction in $k_{\varepsilon,f}$ became less pronounced with a further increase in

Table 5
Summary of referenced specimen results in Figs. 12, 13, 15.

Group	Paper	Number of specimens	Concrete age (day)	f'_{co} (MPa)	Dimensions of cylinder (mm)	Details of FRP confinement
G6-U85-D28	Lim and Ozbakkaloglu [27]	3	28	84.5	152.5 × 305	6 layers of GFRP
G6-U85-D61	Lim and Ozbakkaloglu [27]	3	61	84.8		
C5-U103-D77	Vincent and Ozbakkaloglu [17]	3	77	102.5	152 × 305	5 layers of CFRP
C5-U103-D102	Vincent and Ozbakkaloglu [17]	3	102	102.5		
A6-U110-D48	Ozbakkaloglu and Vincent [16]	6	47–48	104.5	152.5 × 305	6 layers of AFRP
	& Lim and Ozbakkaloglu [27]	3	48	109.8		
A6-U110-D358	Lim and Ozbakkaloglu [27]	3	358	113.5		
C2-C41-D450	Saenz and Pantelides [1]	3	439–450	40.3	152 × 304	2 layers of CFRP
C2-C41-D900	Saenz and Pantelides [1]	3	886–900	41.7		
G1-C41-D450	Saenz and Pantelides [1]	3	439–450	40.3	152 × 304	1 layer of GFRP
G1-C41-D900	Saenz and Pantelides [1]	3	886–900	41.7		

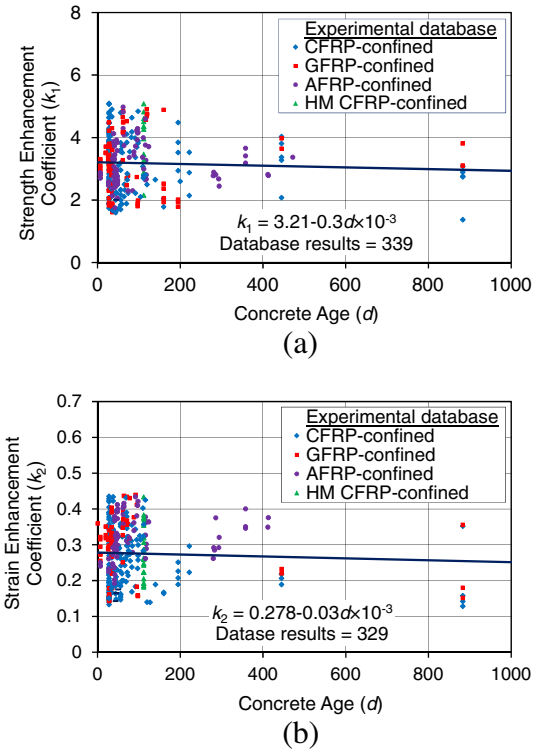

Fig. 14. Variations of: (a) strength enhancement coefficient (k_1); and (b) strain enhancement coefficient (k_2) with concrete age (d).

concrete age from 28 to 358 days, as illustrated in Fig. 15(b). In Fig. 15(c), no notable trend of the variation of $k_{\varepsilon,f}$ values can be seen from the change of concrete age from 450 to 900 days. These observations suggest that, for concretes of same strength, an increase in concrete age results in a reduction in the hoop rupture strain of FRP jackets. However, this effect becomes less pronounced when the concrete age reaches a certain threshold. This reduction can be attributed to the previously discussed influence of concrete age on concrete cracking pattern and resulting brittleness, as was illustrated in Figs. 2–4. As a result of the change in the concrete cracking pattern from heterogenic microcracks to localized macrocracks, the hoop strain distribution in the circumference of the FRP jacket becomes less uniform, which results in a lower recorded average rupture strain. This change in the concrete cracking pattern, however, becomes less pronounced with a further increased concrete age, as can be seen from the more subtle changes in the $k_{\varepsilon,f}$ values of the higher age specimens in Fig. 15(b) and (c), which suggests that concrete brittleness remains unchanged after a certain concrete age.

3.4. Axial strain measurement methods

As was previously discussed in Ozbakkaloglu and Lim [19], the recorded ultimate axial strains (ε_{cu}) are highly sensitive to the type of instrumentation used in their measurement. In the present study, factors causing difference between the axial strains obtained from LVDTs mounted at mid-height of the specimens (AML) and LVDTs mounted along the entire height of the specimens (AFL) were experimentally investigated. An example comparison is shown in Fig. 16, which illustrates the typical stress–strain curves of the NSC and HSC specimens obtained using the two different measurement methods. As evident from the figure, for the NSC specimens, the difference between the strains obtained from the two measurement methods is minimal. On the other hand, this difference is significant for the HSC specimens. Table 6 presents the ultimate axial

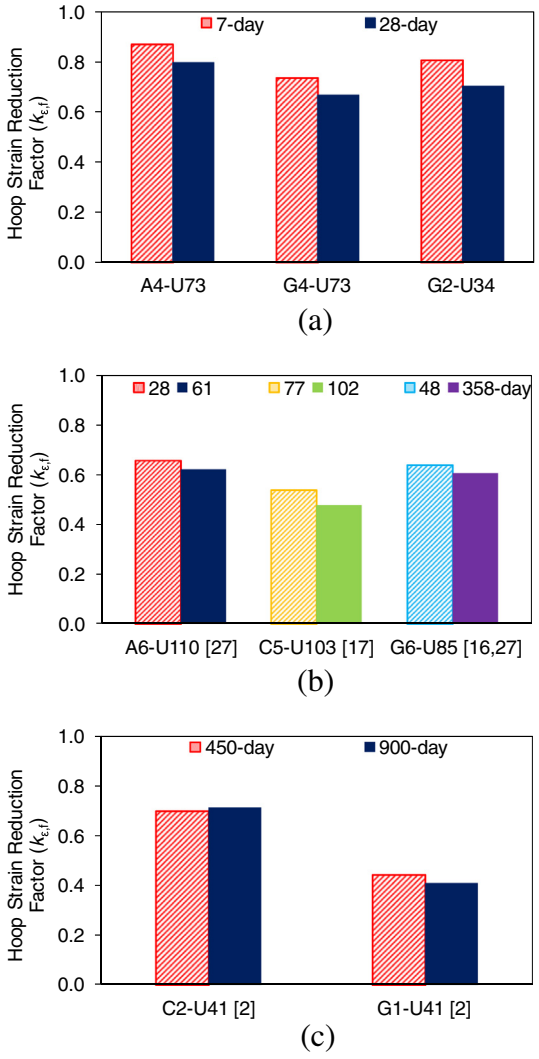

Fig. 15. Variations of hoop rupture strain reduction factor ($k_{\varepsilon,f}$) with concrete age: (a) 7–28 days; (b) 28–358 days; and (c) 450–900 days.

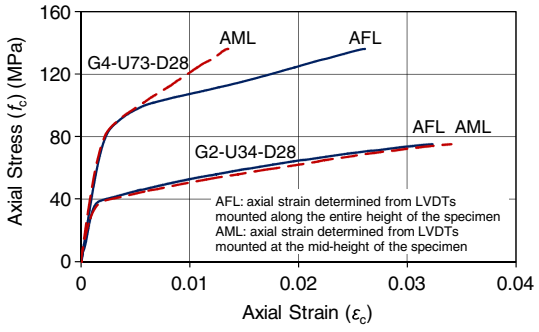

Fig. 16. Influence of instrumentation arrangements on axial stress–strain curves.

strains (ε_{cu}) of specimens recorded using the two measurement methods. Fig. 17(a) shows the comparison of the difference between the axial strains obtained from LVDTs mounted at mid-height of the specimens (AML) and those mounted along the entire height of the specimens (AFL), defined as AML/AFL ratio, with a change in unconfined concrete strength (f'_{co}). As evident from the figure, the difference between AML and AFL increases with an increase in unconfined concrete strength (f'_{co}). This, once again, can be attributed to the change in the concrete cracking pattern

Table 6
Comparison of axial strains measured by different methods.

Specimen	Concrete batch	Average f'_{co} (MPa)	Average ε_{cu} (%)		AML/AFL
			AFL	AML	
A4-U73-D7	B1	70.0	2.12	1.65	0.78
A4-U73-D28	B2	74.9	1.90	1.15	0.61
G4-U73-D7	B3	69.5	2.41	1.33	0.55
G4-U73-D28	B4	74.1	2.68	1.39	0.52
G2-U34-D7	B5	32.3	3.19	3.23	1.01
G2-U34-D28	B6	34.7	3.42	3.53	1.03

AFL: axial strain determined from LVDTs mounted along the entire height of the specimen.
AML: axial strain determined from LVDTs mounted at the mid-height of the specimen.

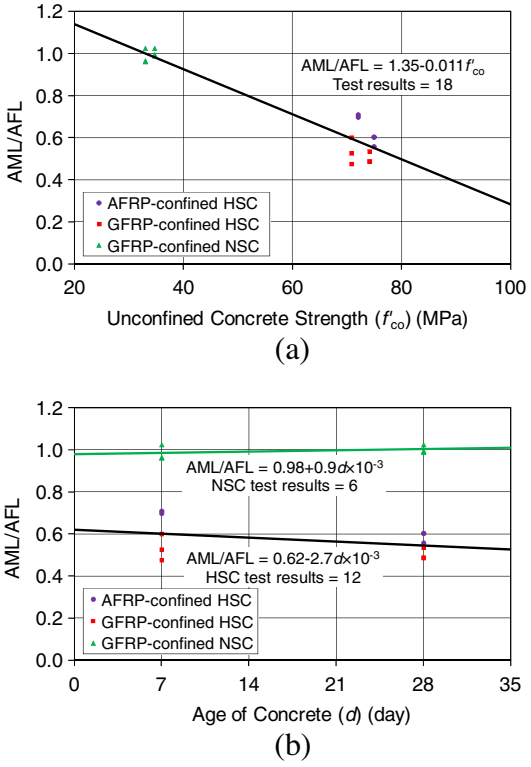

Fig. 17. Variation of AML/AFL ratio with: (a) unconfined concrete strength (f'_{co}); and (b) age of concrete (d).

from microcracks to macrocracks as a result of the increased concrete brittleness with an increase in concrete strength. Detailed discussions on this phenomenon can be found in Ozbakkaloglu and Lim [19] and Lim and Ozbakkaloglu [27].

Closer investigation of the result of the present study indicates that the AML/AFL ratio is also influenced by the age of concrete. This is evident from Fig. 17(b), which shows that the AML/AFL ratio reduces slightly with an increase in the age of the HSC specimens. This variation in the AML/AFL ratio can also be attributed to the change in the concrete cracking pattern [19,27], with larger crack formations observed in specimens with a higher age, as was previously shown in Figs. 2 and 3. These observations indicate that both the unconfined concrete strength and concrete age of FRP-confined concrete influence the concrete cracking behavior, which in turn affect the relative measurements obtained from the two axial strain measurement method. Therefore, when reporting results of experimental studies it is important to specify the type of instrumentation used in the measurement of axial strains to allow an accurate interpretation of the reported strain data.

4. Conclusions

This paper has presented the results of an experimental study on the influence of concrete age on the axial compressive behavior of FRP-confined NSC and HSC. Based on the results and discussions presented in the paper, the following conclusions can be drawn:

1. For a given unconfined concrete strength, the change in concrete age does not significantly alter the ultimate condition of FRP-confined concrete with a concrete age up to 28 days. On the other hand, in the longer term, the compressive strength and the ultimate axial strain of FRP-confined concrete tend to decrease slightly with an increase in the concrete age.
2. The transition regions of stress–strain curves of FRP-confined concrete are observed to be sensitive to the change in concrete age, with specimens tested at a higher age exhibiting curves with smaller transition radii. This observed change has been shown to be a result of the change in the concrete cracking pattern, from microcrack to macrocrack formation, as the concrete age increases. This change in the cracking pattern results in a more rapid concrete expansion and hence increases the concrete dilation rate at the transition region.
3. The hoop rupture strains of FRP jackets decrease with an increase in concrete strength. Furthermore, in specimens with similar unconfined concrete strengths, the hoop rupture strain of FRP also decreases with an increase in concrete age. However, this effect becomes less pronounced when the concrete age reaches a certain threshold.
4. The difference between the axial strains obtained from LVDTs mounted at mid-height of the specimen (AML) and those mounted along the entire specimen height (AFL) increases with an increase in the concrete strength. As a result, a significant difference exists between AML and AFL of HSC specimens. For the HSC specimens with similar unconfined concrete strengths, this difference tends to further increase with an increase in the concrete age. On the other hand, no notable difference exists in the axial strains of NSC specimens obtained from these two measurement methods.

References

[1] Toutanji HA. Durability characteristics of concrete columns confined with advanced composite materials. Compos Struct 1999;44(2–3):155–61.
[2] Saenz N, Pantelides CP. Short and medium term durability evaluation of FRP-confined circular concrete. J Compos Constr 2006;10(3). 244-153.
[3] Walker RA, Karbhari VM. Durability based design of FRP jackets for seismic retrofit. Compos Struct 2007;80(4):553–68.
[4] Erdil B, Akyuz U, Yaman IO. Mechanical behavior of CFRP confined low strength concretes subjected to simultaneous heating–cooling cycles and sustained loading. Mater Struct 2012;45(1–2):223–33.
[5] Hadi MNS, Louk Fanggi BA. Behaviour of FRP confined concrete cylinders under different temperature exposure. In: Proceedings of the 6th international conference on bridge maintenance, safety and management, Stresa, Lake Maggiore, Italy; 2012.
[6] Robert M, Fam A. Long-term performance of GFRP tubes filled with concrete and subjected to salt solution. J Compos Constr 2012;16(2):217–24.
[7] Naguib W, Mirmiran A. Time-dependent behavior of fiber-reinforced polymer-confined concrete columns under axial loads. ACI Struct J 2002;99(2):142–8.
[8] Theriault M, Pelletier MA, Khayat K, Al Chami G. Creep performance of CFRP confined concrete cylinders. In: Proceedings of the 6th international symposium on FRP reinforcement for concrete structures, Singapore; 2003.
[9] Berthet JF, Ferrier E, Hamelin P, Al Chami G, Theriault M, Neale KW. Modelling of the creep behavior of FRP-confined short concrete columns under compressive loading. Mater Struct 2006;39(1):53–62.
[10] Kaul R, Ravindrarajah RS, Smith ST. Deformational behavior of FRP confined concrete under sustained compression. In: Proceedings of the 3rd international conference on FRP composites in civil engineering, Miami, Florida; 2006.
[11] Demir C, Kolcu K, Ilki A. Effects of loading rate and duration on axial behavior of concrete confined by fiber-reinforced polymer sheets. J Compos Constr 2010;14(2):146–51.

[12] Wang YF, Ma YS, Zhou L. Creep of FRP-wrapped concrete columns with or without fly ash under axial load. Constr Build Mater 2011;25(2):697–704.
[13] Lim JC, Ozbakkaloglu T. Stress–strain model for normal- and light-weight concretes under uniaxial and triaxial compression. Constr Build Mater 2014;71:492–509.
[14] ASTM-D3039. Standard test method for tensile properties of polymer matrix composite materials. D3039/D3039M-08, West Conshohocken, PA; 2008.
[15] Ozbakkaloglu T, Akin E. Behavior of FRP-confined normal- and high-strength concrete under cyclic axial compression. J Compos Constr, ASCE 2012;16(4):451–63.
[16] Ozbakkaloglu T, Vincent T. Axial compressive behavior of circular high-strength concrete-filled FRP tubes. J Compos Constr, ASCE 2013;18(2):04013037.
[17] Vincent T, Ozbakkaloglu T. Influence of concrete strength and confinement method on axial compressive behavior of FRP-confined high- and ultra high-strength concrete. Compos B 2013;50:413–28.
[18] Lim JC, Ozbakkaloglu T. Confinement model for FRP-confined high-strength concrete. J Compos Constr, ASCE 2014;17(5):1–19.
[19] Ozbakkaloglu T, Lim JC. Axial compressive behavior of FRP-confined concrete: experimental test database and a new design-oriented model. Compos B 2013;55:607–34.
[20] Harries KA, Carey SA. Shape and "gap" effects on the behavior of variably confined concrete. Cem Concr Res 2003;33(6):881–90.
[21] De Lorenzis L, Tepfers R. Comparative study of models on confinement of concrete cylinders with fiber-reinforced polymer composites. J Compos Constr 2003;7(3):219–37.
[22] Lam L, Teng JG. Ultimate condition of fiber reinforced polymer-confined concrete. J Compos Constr, ASCE 2004;8(6):539–48.
[23] Ozbakkaloglu T, Lim JC, Vincent T. FRP-confined concrete in circular sections: review and assessment of stress–strain models. Eng Struct 2013;49:1068–88.
[24] Vincent T, Ozbakkaloglu T. Influence of fiber orientation and specimen end condition on axial compressive behavior of FRP-confined concrete. Constr Build Mater 2013;47:814–26.
[25] Lim JC, Ozbakkaloglu T. Lateral strain-to-axial strain relationship of confined concrete. J Struct Eng, ASCE, 2014. http://dx.doi.org/10.1061/(ASCE)ST.1943-541X.0001094.
[26] Lim JC, Ozbakkaloglu T. Hoop strains in FRP-confined concrete columns: experimental observations. Mater Struct 2014. http://dx.doi.org/10.1617/s11527-014-0358-8.
[27] Lim JC, Ozbakkaloglu T. Influence of silica fume on stress–strain behavior of FRP-confined HSC. Constr Build Mater 2014;63:11–24.